A&A 666, A185 (2022)
https://doi.org/10.1051/0004-6361/202244097


Astronomy & Astrophysics

# Photometric behavior of Ryugu's NIR spectral parameters

A. Longobardo[1], E. Palomba[1,2], A. Galiano[1], F. Dirri[1], A. Zinzi[2], M. D'Amore[3], D. Domingue[4], K. Kitazato[5], Y. Yokota[6], S. E. Schroeder[3], T. Iwata[6], M. Matsuoka[6], T. Hiroi[7], D. Takir[8], T. Nakamura[9], M. Abe[5], M. Ohtake[5], S. Matsuura[10], S. Watanabe[6,11], M. Yoshikawa[6], T. Saiki[6], S. Tanaka[6], T. Okada[6], Y. Yamamoto[6], Y. Takei[6], K. Shirai[6], N. Hirata[5], N. Hirata[12], K. Matsumoto[13], and Y. Tsuda[5]

[1] INAF-IAPS, Rome, Italy
e-mail: andrea.longobardo@inaf.it
[2] ASI-SSDC, Rome, Italy
[3] German Aerospace Center, Institute of Planetary Research, Berlin, Germany
[4] PSI, Tucson, AZ, USA
[5] University of Aizu, Aizu-Wakamatsu 965-8580, Fukushima, Japan
[6] ISAS-JAXA, 3-1-1 Yoshino-dai, Chuo-ku, Sagamihara, Kanagawa, Japan
[7] Department of Earth, Environmental and Planetary Sciences, Brown University, Providence, RI 02912, USA
[8] Jacobs/NASA Johnson Space Center, USA
[9] Tohoku University, Miyagi, Japan
[10] Kwansei Gakuin University, Hyogo, Japan
[11] Nagoya University, Nagoya 464-8601, Japan
[12] Kobe University, Kobe 657-8501, Japan
[13] National Astronomical Observatory of Japan, Mitaka 181-8588, Japan

Received 23 May 2022 / Accepted 22 August 2022

**ABSTRACT**

*Context.* JAXA's Hayabusa2 mission rendezvoused the Ryugu asteroid for 1.5 years to clarify the carbonaceous asteroids' record for Solar System origin and evolution.
*Aims.* We studied the photometric behavior of the spectral parameters characterizing the near-infrared (NIR) spectra of Ryugu provided by the Hayabusa2/NIRS3 instrument, that is to say 1.9 μm reflectance, 2.7 and 2.8 μm band depths (ascribed to phyllosilicates), and NIR slope.
*Methods.* For each parameter, we applied the following empirical approach: (1) retrieval of the equigonal albedo by applying the Akimov disk function (this step was only performed for the reflectance photometric correction); (2) retrieval of the median spectral parameter value at each phase angle bin; and (3) retrieval of the phase function by a linear fit.
*Results.* Ryugu's phase function shows a steepness similar to Ceres, according to the same taxonomy of the two asteroids. Band depths decrease with increasing phase angle: this trend is opposite to that observed on other asteroids explored by space missions and is ascribed to the very dark albedo. NIR and visible phase reddening are similar, contrary to other asteroids, where visible phase reddening is larger: this could be due to surface darkness or to particle smoothness. Albedo and band depths are globally uncorrelated, but locally anticorrelated. A correlation between darkening and reddening is observed.

**Key words.** minor planets, asteroids: general – minor planets, asteroids: individual: Ryugu – methods: data analysis – techniques: photometric – techniques: spectroscopic

## 1. Introduction

Ryugu is the near-Earth, C-type asteroid selected as the target of the JAXA/Hayabusa2 sample return mission (Watanabe et al. 2017; Tachibana 2021) to clarify the C-type asteroids' record for Solar System origin and evolution, as well as the link between these asteroids and the carbonaceous chondrites (i.e., the most primitive meteorite group). Hayabusa2 rendezvoused with Ryugu for about 1.5 yr (i.e., from June 2018 to November 2019), observed the asteroid by means of an orbiter and two rovers, performed two touchdown operations (TD-1 on 21 February 2019 and TD-2 on 11 July 2019) with related sampling, as well as an artificial impact experiment (5 April 2019, Arakawa et al. 2020).

The mission determined that Ryugu is a rubble-pile asteroid, as suggested from its small size (mean radius ~450 m, Watanabe et al. 2019; and equatorial radius ~500 m, Suguta et al. 2019), low density (i.e., $1.19 \pm 0.03$ g cm$^{-3}$, Watanabe et al. 2019), top shape with an equatorial ridge (Watanabe et al. 2019), and high number density of boulders larger than 20 m (Suguta et al. 2019). Similar properties have also been found for the asteroid Bennu, which is the target of the NASA/OSIRIS-REx sample return mission (Lauretta et al. 2015, 2021), suggesting a rubble-pile origin even for this asteroid (e.g., Scheeres et al. 2019).

Ryugu's optical as well as visible and near-infrared (NIR) spectral properties have been studied from the Optical Navigation Camera (ONC, Kameda et al. 2017) and the Near-Infrared Spectrometer (NIRS3, Iwata et al. 2017). Ryugu is one of the darkest planetary objects observed so far from space missions, with a geometric albedo of ~0.043 (Suguta et al. 2019). It is weakly hydrated, as suggested from the shallow O-H stretching bands centered at 2.72 and 2.8 μm, respectively (Kitazato et al. 2019; Galiano et al. 2020).

Ryugu surface's optical and physical properties have also been studied by analyzing its photometric behavior, that is the

reflectance trend as a function of illumination and observation angles. Tatsumi et al. (2020) studied Ryugu's global photometric properties by applying the Hapke model to the combined ONC and ground-based data. They obtained an average geometric albedo of 0.04 and an average reflectance factor of 0.018 in the $v$ band (centered at 0.55 μm). Moreover, they retrieved a visible phase reddening (i.e., increase in the visible spectral slope with a phase angle) of $(2.0 \pm 0.3) \times 10^{-3}\,\mu m^{-1} deg^{-1}$ and found a general correlation between darkening and reddening (with a few exceptions). Pilorget et al. (2021) applied the Hapke model to NIRS3 data and found that Ryugu's photometric properties in the NIR range are quite constant across the surface. However, darker areas associated with a slightly deeper 2.72 μm band and a few brighter areas were observed.

In this work, we study the photometric properties of Ryugu by applying a statistical, semiempirical model, as has already been done for other small bodies, such as Vesta (Longobardo et al. 2014), Lutetia (Longobardo et al. 2016), 67P/Churyumov-Gerasimenko (Longobardo et al. 2017), and Ceres (Longobardo et al. 2019). This approach provides complementary information with respect to the Hapke model, such as the photometric behavior of spectral parameters (spectral slope and band depths) and related scientific implications.

Section 2 introduces the NIRS3 instrument and the dataset considered for this work. The studied spectral parameters are defined in Sect. 3. The photometric model is explained in Sect. 4, with results given in Sect. 5 and discussed in Sect. 6. Finally, conclusions are summarized in Sect. 7.

## 2. Data

We used the data provided by the NIRS3 point spectrometer (Iwata et al. 2017) acquired between the two touchdowns. After the second touchdown, a new radiometric calibration was performed (Riu et al. 2021); therefore, we limited our analysis to the spectra calibrated with the same instrument transfer function.

The NIRS3 spectral range is 1.8–3.2 μm, with a spectral resolution of 18 nm and a field of view of 0.1°. The spatial resolution in the considered dataset varies from a few to about 10 m pixel$^{-1}$, while the phase angle range is 15–40°. The phase interval considered for studying small bodies' photometry is generally wider, especially for a case in which the study is based on a statistical analysis of the dataset. Therefore, we redefined the photometric parameters used to compare small bodies, as described in Sect. 4. All the spectra were corrected for the thermal contribution by applying the procedure described by Kitazato et al. (2019).

## 3. Tools

The photometric correction was applied on the radiance factor at 1.9 μm (hereafter referred to as reflectance), on hydration band depths at 2.72 μm (hereafter 2.7 μm) and 2.8 μm, and on the infrared spectral slope between 1.9 and 2.5 μm. All these spectral parameters are important descriptors of the regolith composition, granulometry, and weathering; therefore, their photometric correction is a fundamental data reduction operation. Definitions of these parameters are described by Galiano et al. (2020) and summarized below.

The reflectance at 1.9 μm was calculated as the average between the three NIRS3 spectral bands closest to the considered wavelength, so as to minimize signal oscillations and therefore maximize the signal-to-noise ratio. To define the band shoulders, we smoothed the spectra by replacing the reflectance at each wavelength with the reflectance averaged on the three closest NIRS3 spectral bands. Then, for both bands we defined the left and right shoulder as the maximum reflectance in the range 2.50–2.65 μm and 2.85–2.95 μm, respectively. The spectral continuum is the straight line connecting the two shoulders. The band center was defined as the band minimum after the continuum removal: it was calculated in the range 2.70–2.75 μm for the 2.7 μm band and in the range 2.80–2.85 μm for the 2.8 μm band. Band depths, BD, were defined by adopting the definition by Clark & Roush (1984), that is

$$\mathrm{BD} = 1 - \frac{R_c}{R_{cont}} \tag{1}$$

where $R_c$ and $R_{cont}$ are the reflectance and the continuum at the band center. Spectral slope $S_{IR}$ was also defined on smoothed spectra and calculated as

$$S_{IR} = \frac{R_{2.5} - R_{1.9}}{R_{2.5}(2.5 - 1.9)}, \tag{2}$$

where $R_\lambda$ are the reflectance at the wavelengths $\lambda$ and $S_{IR}$ was calculated in μm$^{-1}$.

## 4. Method

### 4.1. Preliminary operations

We first verified the absence of systematic effects, which may affect the retrieved photometric functions, by investigating three issues: (1) residuals of the thermal emission removal procedure that could affect the spectra longward of 2.5 μm (Kitazato et al. 2019), and therefore the retrieval of the band depths (Galiano et al. 2020); (2) the temperature influence on the spectral slope (Riu et al. 2021), which could be due to inaccuracies of the surface temperature retrieval and to the removal of thermal contribution; and (3) bad spectra collected by NIRS3 just after the TD1 (Kitazato, priv. comm.).

Concerning the first issue, we applied the procedure by Galiano et al. (2020) to evaluate the thermal emission removal residuals. To this end, the reflectance behavior was studied as a function of the temperature at two wavelengths, one inside (i.e., 1.9 μm) and one outside (i.e., 3.0 μm) the thermal emission region. In fact, the reflectance ratio $R_{3.0}/R_{1.9}$ has a slight dependence on the temperature (Fig. 1), suggesting that an overcorrection for the thermal contribution may be present. Nevertheless, the reflectance variation is no larger than 3% (i.e., between 1.03 and 1.06), which corresponds to an albedo variation of about 0.001. This variation can be considered negligible because of the following: (a) it is much lower than the reflectance spread observed on Ryugu (Galiano et al. 2020); (b) it is similar or lower than the uncertainties introduced from the photometric correction procedure (Sect. 4.2); and (c) it is much lower than the reflectance variation with observation angles. In conclusion, if an overcorrection of the thermal contribution is present on the NIRS3 spectra, it does not affect the results.

Concerning the second issue, Riu et al. (2021) found that the spectral slope between 1.9 and 2.5 μm increases slightly with temperature (i.e., <1% per degree). This variation is much smaller than the spectral slope variation with the phase angle (Sect. 5). In addition, even if it was significant, it would introduce a trend opposite to that observed (a spectral slope increase with the phase angle). Therefore, the phase behavior observed on the spectral slope (Sect. 5) is not affected by this temperature dependence. Concerning the third issue, the statistical analysis adopted

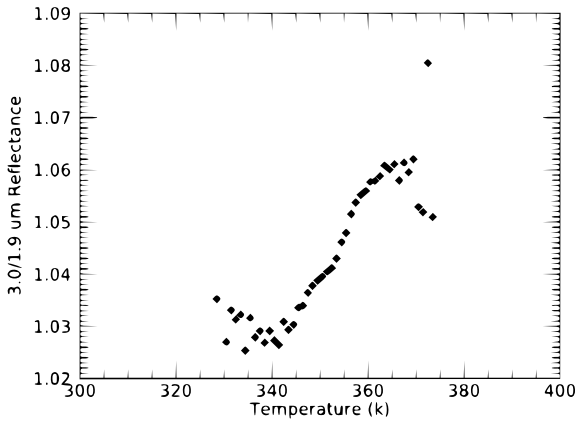


**Fig. 1.** Ratio between the reflectance calculated at two wavelengths (3.0 and 1.9 μm) as a function of temperature.

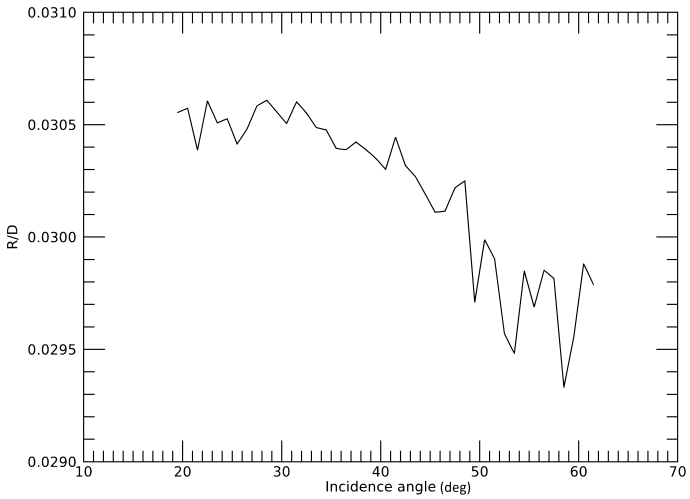


**Fig. 2.** Equigonal albedo at 1.9 μm obtained by applying the Akimov disk function as a function of the incidence angle. The residual variation is about 3%.

and explained in the next subsection automatically excludes all the bad spectra, which are not statistically significant.

### 4.2. Retrieval of photometric behaviors

The method used to retrieve the photometric behavior of all spectral parameters introduced in Sect. 3 was applied in the three following steps:

1. The removal of topography influence (i.e., influence from incidence and emission) by applying the Akimov disk function (Shkuratov et al. 1999) is defined as follows:

$$D(\beta,\gamma,\phi) = \cos\frac{\phi}{2}\cos\left[\frac{\pi}{\pi-\phi}\left(\gamma-\frac{\phi}{2}\right)\right]\frac{(\cos\beta)^{\frac{\phi}{\pi-\phi}}}{\cos\phi}, \quad (3)$$

where $\gamma = \arctan frac\cos i - \cos e\cos\phi\ \cos e\cos\phi$ is the photometric longitude and $\beta = \arccos\frac{\cos e}{\cos\gamma}$ is the photometric latitude.

In previous studies on the photometry of small, dark bodies (Longobardo et al. 2014, 2016, 2017, 2019), several disk functions were tested, and the Akimov disk function was selected as the best one in all cases. For this reason, we considered only this disk function and verified its goodness a posteriori.

Because the disk function is a multiplying term of the reflectance, this step was only applied to the reflectance, $R$, photometric correction: in this case we obtained the equigonal albedo $R/D$. We did not apply this step for parameters defined as a reflectance ratio (band depths and spectral slope).

2. The second step involved the retrieval of the median spectral parameter behavior as a function of the phase angle (phase angle bins of 1° were considered). In the case of the 1.9 μm reflectance, we considered the phase behavior of the equigonal albedo.

3. The last step involved a phase function retrieval by a least squares fit.

### 4.3. Photometric parameters

To compare the photometric behavior of small bodies, Longobardo et al. (2016, 2017) defined two spectral parameters: $R30$, that is the radiance factor in the visible range at a phase angle of 30°, and PCS (phase curve slope), that is the phase function steepness between 20° and 60° phase angles. We note that PCS = $1 - R60/R20$, where $R60$ and $R20$ are the radiance factors in the visible range at 60° and 20° phase angles, respectively.

In this case, we adapted these definitions for the infrared spectral range and for the available phase angle range. Therefore, our photometric parameters were redefined as follows: $R30$ is the NIR reflectance and PCS is the phase curve steepness between 15° and 40° phase angles, that is PCS = $1 - R40/R15$, where $R40$ and $R15$ are the radiance factors in the NIR range at 40° and 15° phase angles, respectively.

The photometric parameters defined above can only be calculated for three asteroids explored by space missions, that is Eros (Clark et al. 2002), Vesta (Longobardo et al. 2014), and Ceres (Longobardo et al. 2019). A comparison between the photometric parameters of the four asteroids was finally performed.

## 5. Results

Figure 2 shows the 1.9 μm equigonal albedo obtained by applying the Akimov disk function as a function of the incidence angle. A slight decreasing trend is still observable, but residual variations are lower than 3%, that is less than 0.001, which, as discussed in Sect. 4.1 is considered insignificant. The $R/D$ variation with the emission angle is even lower. Based on this and on photometric studies on other dark, small bodies (Longobardo et al. 2017, 2019), we did not test other disk functions and considered the Akimov one.

The phase function is shown in Fig. 3. Due to the narrow phase angle considered, we calculated the phase function by applying a linear fit. The phase function slope obtained is $-(4.1 \pm 0.1) \times 10^{-4}\mathrm{deg}^{-1}$.

In Table 1, we show the photometric parameters of Ryugu, Ceres (Longobardo et al. 2019), Eros (Clark et al. 2002), and Vesta (Longobardo et al. 2014), as defined in Sect. 4.3. The PCS of the four asteroids was calculated in the same phase angle range, that is between 15° and 40°.

The 2.7 and 2.8 μm band depths show a similar decreasing trend with an increasing phase angle (Fig. 4). The decreasing rate of the two band depths is $-(5.3 \pm 0.8) \times 10^{-4}\mathrm{deg}^{-1}$ and $-(5.0 \pm 0.9) \times 10^{-4}\mathrm{deg}^{-1}$, respectively.

The NIR spectral slope as a function of the phase angle is shown in Fig. 5. The slope of the linear fit modeling this trend is the phase reddening. We applied a linear fit for an easy comparison with other small bodies. In fact, the $S_{IR}$ behavior seems to be

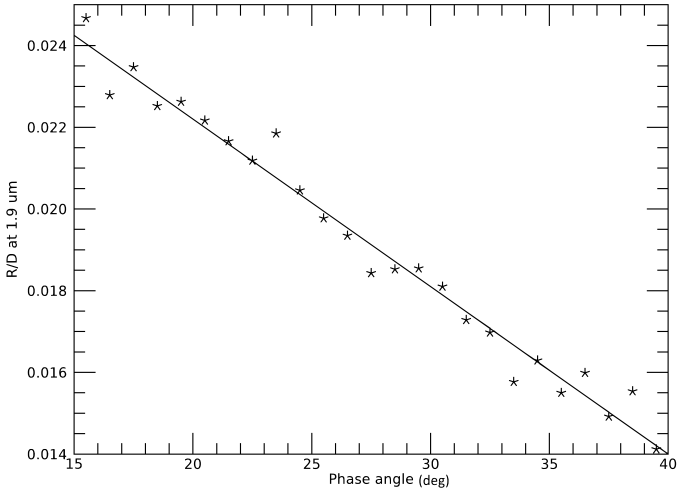


**Fig. 3.** Equigonal albedo at 1.9 μm as a function of the phase angle (error bars are not shown for clarity, but are included within the symbols). The straight line is Ryugu's phase function that was retrieved.

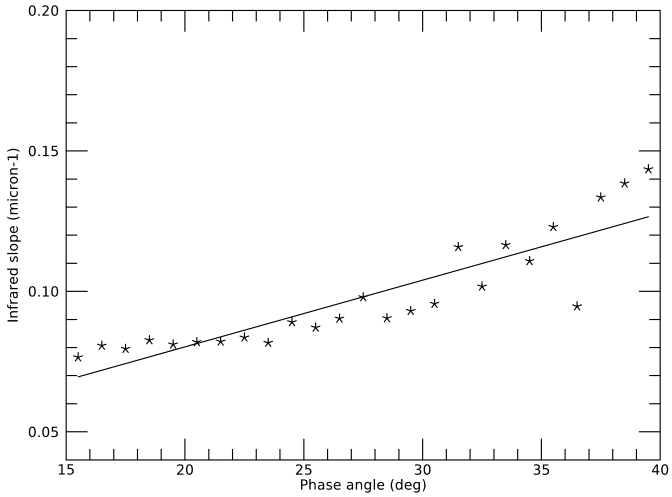


**Fig. 5.** Infrared spectral slope as a function of the phase angle and linear fit reproducing its behavior. Error bars are not shown for clarity, but are included within the symbols' size.

**Table 1.** Photometric parameters calculated for the asteroids with an available NIR disk-resolved phase function.

| Asteroid | Spectral type | $R30$ | PCS (%) | Reference |
|---|---|---|---|---|
| Ryugu | C | 0.02 | $50 \pm 2$ | This work |
| Ceres | C | 0.03 | $52 \pm 5$ | Longobardo et al. (2019) |
| Eros | S | 0.13 | $41 \pm 3$ | Clark et al. (2002) |
| Vesta | V | 0.16 | $41 \pm 1$ | Longobardo et al. (2014) |

**Notes.** The uncertainties on $R30$ are lower than 0.01.

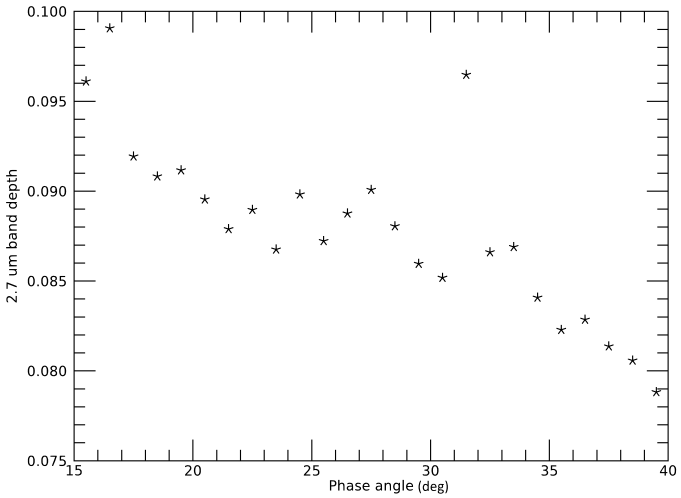


**Fig. 4.** Band depth at 2.7 μm as a function of the phase angle. Error bars are not shown for clarity, but are included within the symbols' size (except the values at 31° and 35°, which have an uncertainty larger than 0.01). The behavior of the 2.8 μm band depth is similar.

better reproduced by a second order polynomial. We ascribe this to the small phase angle range considered. However, the $R^2$ value of the linear fit is 0.8, which is better than $R^2$ obtained for other bodies (e.g., 67P/Churyumov-Gerasimenko, Longobardo et al. 2017).

## 6. Discussion

### 6.1. NIR phase functions: Comparative analysis

Even if the comparison of photometric parameters shown in Table 1 involves only four asteroids, we can clearly discern two families: (1) C-type asteroids (Ceres and Ryugu), which are characterized by a low albedo and a higher PCS, and (2) bright asteroids (Vesta and Eros), with a lower PCS. Therefore, Ryugu's photometric behavior is what is to be expected for a dark, C-type body, where multiple scattering (i.e., the main factor responsible of phase function flattening) has a negligible role.

### 6.2. Band depths

The band depth decreasing with increasing phase angle observed on Ryugu had never been observed on other dark bodies explored by space missions before. The band depth behavior as a function of the phase angle for different small bodies is summarized in Table 2.

In the case of Vesta, the band depth increases with phase more steeply with an increasing opaque amount (i.e., with decreasing albedo): in Vesta's bright terrains, the band depth's increasing rate with phase is lower than for dark terrains. Longobardo et al. (2014) ascribed this to the more important role of multiple scattering in bright terrains, which redistributes radiation at different phase angles and flattens the phase curve.

A different explanation should be considered for dark bodies (i.e., albedo lower than 0.01) because, in this case, the multiple scattering role is negligible. Moreover, the band depth versus phase trend has the opposite behavior with respect to bright asteroids, because it is steeper for greater albedos. Longobardo et al. (2017) ascribed the band depth's photometry on Churyumov-Gerasimenko to the surface darkness: when the albedo decreases, it suppresses not only the band, but also its photometric behavior, that is to say the band depth is phase-independent.

When the albedo further decreases (as is the case of Ryugu), we could observe a band depth decreasing with phase due to

**Table 2.** Photometric behavior of NIR band depths in small bodies explored by space missions.

| Body | Albedo | Band depth vs. phase(*) | Reference |
|---|---|---|---|
| Vesta | 0.40 | Increasing | Longobardo et al. (2014) |
| Ceres | 0.09 | Increasing | Longobardo et al. (2019) |
| 67P/Churyumov-Gerasimenko | 0.06 | Constant | Longobardo et al. (2017) |
| Ryugu | 0.04 | Decreasing | This work |

**Notes.** (*)The band depths considered include 0.9 and 1.9 μm for Vesta (due to pyroxenes), 2.7 and 3.1 μm for Ceres (due to ammoniated phyllosilicates), 3.2 μm for 67P/Churyumov-Gerasimenko (due to organics and ammonium salts), and 2.7 and 2.8 μm for Ryugu (due to phyllosilicates).

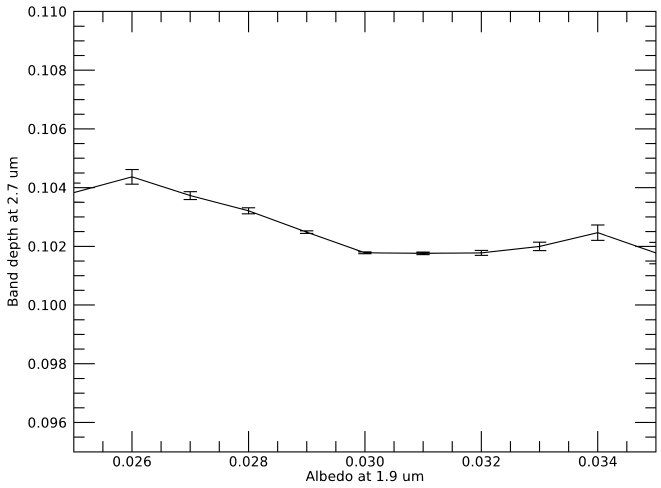


**Fig. 6.** Photometrically corrected 2.7 μm band depth as a function of the 1.9 μm albedo. The behavior of the 2.8 μm band is similar.

the combination of the following effects: (a) I/F decreases more steeply with the phase angle; and (b) darkening tends to suppress absorption bands (with an equal band carrier abundance), as is generally observed on planetary surfaces. This would generate the observed photometric trend. While this interpretation is not definitive, it is consistent with the photometric behavior of the Murchison meteorite, which is darker than Ryugu (being its albedo 0.03) and still shows a band depth decreasing trend with the phase (Cloutis et al. 2018).

This interpretation is independent of the composition of the band carrier (being related only to the average albedo) and is related to a general behavior. It does not consider particular surface physical properties, such as grain size and roughness.

### 6.3. Albedo versus band depth

Pilorget et al. (2021) conclude that 2.7 and 2.8 μm bands are deeper in dark regions. We related the photometric corrected band depths and infrared albedo, as shown in Fig. 6.

We are still able to observe a band deepening at decreasing albedo, but this is very slight (less than 2%), lower than that observed by Pilorget et al. (2021), and limited to albedo values lower than 0.03. However, the two conclusions are not contradictory because of the different approaches used by two works. In fact, Pilorget et al. (2021) considered mean band depth values (instead of median ones, as we do) and studied the local correlation between albedo and band depths, instead of a global one. In particular, the areas selected by Pilorget et al. (2021) are among the darkest ones of Ryugu and this amplifies the observed band deepening with decreasing albedo. Therefore, while we observe that the band depth is quite independent of the albedo, a local anticorrelation is not excluded.

**Table 3.** Visible and infrared phase reddening measured on dark bodies explored by space missions.

| Body | VIS phase reddening ($\times10^{-3}\mu m^{-1}deg^{-1}$) | NIR phase reddening ($\times10^{-3}\mu m^{-1}deg^{-1}$) | References |
|---|---|---|---|
| Ceres | 4.6 | 1.5 | Ciarniello et al. (2017), Longobardo et al. (2019) |
| 67P/CG | 5.4 | 1.5 | Longobardo et al. (2017) |
| Bennu | 1.5 | 0.4(*) | Golish et al. (2021), Zou et al. (2021), Li et al. (2021), Fornasier et al. (2020) |
| Ryugu | 2.0 | 2.1 | Tatsumi et al. (2020), This work |

**Notes.** (*)Average value from the visible to NIR range.

### 6.4. Infrared slope

From the infrared slope phase function (Fig. 5), we retrieved a phase reddening of $(2.1 \pm 0.3) \times 10^{-3}\mu m^{-1}deg^{-1}$. This value is very similar to that found by Tatsumi et al. 2020 on ONC data in the visible range (Table 3). Ceres and 67P instead show a visible phase reddening about 3 times the infrared one (Table 3). In the case of Bennu, the visible phase reddening is very similar to Ryugu (Golish et al. 2021), but average phase reddening from the visible to NIR is about 4 times less (Zou et al. 2021). This suggests that Bennu shows a phase reddening decrease from the visible to NIR, as Ceres and 67P and different than Ryugu (Table 3).

We discuss three possible explanations for this result, two optical and one physical:

*Multiple scattering.* On 67P, the larger, even if weak, multiple scattering in the NIR (evidenced by the higher albedo, Capaccioni et al. 2015) may produce a phase function shallowing (i.e., a decreasing phase reddening) at longer wavelengths, while the multiple scattering role on Ryugu would be the same (i.e., almost null) in the two spectral intervals (similar albedos). This interpretation has two weaknesses: (a) the 67P's PCS is quite constant from 0.5 to 2 μm (Longobardo et al. 2017); and (b) Ceres and Bennu show a similar albedo (e.g., Raponi et al. 2021; Barucci et al. 2020), but different phase reddening values in the two spectral intervals.

*Spectral slope.* Phase reddening could follow spectral slope variations. Ryugu's visible and infrared spectral slopes are similar; whereas, on the other three asteroids, the visible slope is larger (in absolute value) than the infrared one. However, in the case of Bennu, slopes are negative (i.e., blue spectrum, Barucci et al. 2020), which is different than Ceres and 67P.

*Sub-μm roughness.* At the scale of the particle surface, submicron roughness can explain the monotonic phase reddening (Schröder et al. 2014). The different interaction of visible and infrared light with particle roughness can produce a different phase reddening response. In the case of Ryugu, the response is the same in the two spectral intervals, that means visible and infrared light would "see" the same microroughness. This would mean that submicrometric roughness (a) is absent, that is Ryugu particles are smooth, or (b) is present, but does not play a role in light scattering because the internal scattering is killed by the low albedo. Therefore, Ryugu behaves even in the visible range as Ceres and 67P do in the infrared, where the roughness role is minimized. According to this explanation, Bennu should have a regolith particles' roughness, which is different than Ryugu. However, due to their similar formation processes (Michel et al. 2020), this is unlikely.

Nevertheless, we should consider that the obtained phase reddening values could be affected by: the narrow phase angle range considered, in the case of Ryugu, and a segment jump at 0.66 μm (Zou et al. 2021) in the case of Bennu. Our preliminary conclusion is that the weak phase reddening observed on Ryugu from the visible to NIR could be due to its low albedo, while analysis of returned samples will clarify the role of regolith's physical properties.

### 6.5. Albedo versus infrared slope

Photometrically corrected NIR slopes are generally steeper in dark areas and flatter in brighter ones. This confirms the well-known relation between surface darkening and reddening (e.g., Galiano et al. 2020), ascribed to thermal metamorphism and space weathering.

## 7. Conclusions

We studied the photometric behavior of infrared parameters describing the Ryugu spectra. To this end, we applied a semiempirical approach based on a statistical analysis of the Hayabusa2/NIRS3 dataset.

The phase function at 1.9 μm was modeled by combining the Akimov disk function with a linear fit (due to the narrow phase angle interval). From a comparison between asteroids' NIR phase functions, we identified two families: C-type (Ryugu and Ceres) and bright (Eros and Vesta) asteroids.

The 2.72 and 2.8 μm band depths decrease with increasing phase angle, which is different than the behavior observed on other asteroids. This has been ascribed to the dark Ryugu albedo, which mainly suppresses the bands at higher phase angles.

Near-infrared and visible phase reddening are similar, contrary to other small bodies characterized by a larger phase reddening in the visible range. This could be ascribed to the surface darkness, though particle smoothness can play a role: analysis of returned Ryugu (and Bennu) samples can clarify this issue.

Albedo and photometrically corrected band depths are globally uncorrelated. Nevertheless, a local anticorrelation is possible, while a correspondence between darkening and reddening is observed due to thermal metamorphism and space weathering.

*Acknowledgements.* This work is founded by the Italian Space Agency (ASI) and it has been developed under the agreement 2022-12-HH-0. The Hayabusa2 spacecraft was developed and built under the leadership of Japan Aerospace Exploration Agency (JAXA), with contributions from the German Aerospace Center (DLR) and the Center National d'Études Spatiales (CNES), and in collaboration with NASA, Nagoya University, University of Tokyo, National Astronomical Observatory of Japan (NAOJ), University of Aizu, Kobe University, and other universities, institutes, and companies in Japan. We also thank the engineers who contributed to the success of Hayabusa2 operations.

## References

Arakawa, M., Saiki, T., Wada, K., et al. 2020, Science, 368, 67
Barucci, M. A., Hasselmann, P. H., Praet, A., et al. 2020, A&A, 637, L4
Capaccioni, F., Coradini, A., Filacchione, G., et al. 2015, Science, 347, aaa0628
Ciarniello, M., De Sanctis, M.C., Ammannito, E., et al., 2017, A&A, 598, A130
Clark, R. N., & Roush, T. N. 1984, J. Geophys. Res., 89, 6329
Clark, B. E., Helfenstein, P., Bell III, J. F., et al. 2002, Icarus, 155, 189
Cloutis, E. C., Pietrasz, V. B., Kiddell, C., et al. 2018, Icarus, 305, 203
Fornasier, S., Hasselmann, P. H., Deshapriya, J. D. P., et al. 2020, A&A, 644, A142
Galiano, A., Palomba, E., D'Amore, M., et al. 2020, Icarus, 351, 113959
Golish, D. R., DellaGiustina, D. N., Li, J.-Y., et al. 2021, Icarus, 357, 113724
Iwata, T., Kitazato, K., Abe, M., et al. 2017, Space Sci. Rev., 208, 317
Kameda, S., Suzuki, H., Takamatsu, T., et al. 2017, Space Sci. Rev., 208, 17
Kitazato, K., Milliken, R. E., Iwata, T., et al. 2019, Science, 364, 272
Lauretta, D. S., Bartels, A. E., Barucci, M. A., et al. 2015, Meteor. Planet. Sci., 50, 4, 834
Lauretta, D. S., Enos, H. L., Polit, A. T., et al. 2021, In: Sample Return Missions: The Last Frontieer of Solar System Exploration, ed. A. Longobardo (Amsterdam: Elsevier), 163
Li, J.-Y., Zou, X.-D., Golish, D. R., et al. 2021, Planet. Sci. J., 2, 117
Longobardo, A., Palomba, E., Capaccioni, F., et al. 2014, Icarus, 240, 20
Longobardo, A., Palomba, E., Ciarniello, M., et al. 2016, Icarus, 267, 204
Longobardo, A., Palomba, E., Capaccioni, F., et al. 2017, MNRAS, 469, S346
Longobardo, A., Palomba, E., Galiano, A., et al. 2019, Icarus, 320, 97
Michel, P., Ballouz, R.-L., Barnouin, O. S., et al. 2020, Nat Commun., 11, 2655
Pilorget, C., Fernando, J., Riu, L., Kitazato, K., & Iwata, T. 2021, Icarus, 355, 114126
Raponi, A., De Sanctis, M. C., Carrozzo, F. G., et al. 2021, Life, 11, 1
Riu, L., Pilorget, C., Millike, L., et al. 2021, Icarus, 357, 114253
Scheeres, D. J., McMahon, J. W., French, A. S., et al. 2019, Nat. Astron., 3, 352
Schröder, S. E., Mottola, S., Keller, H. U., Raymond, C. A., & Russell, C. T. 2014, Planet. Space Sci., 103, 66
Shkuratov, Y. G., Kreslavski, M. A., Ovcharenko, A. A., et al. 1999, Icarus 141, 132
Sugita, S., Honda, R., Morota, T., et al. 2019, Science, 364, eaaw0422
Tachibana, S. 2021, In: Sample Return Missions: The Last Frontieer of Solar System Exploration, ed. A. Longobardo (Amsterdam: Elsevier), 147
Tatsumi, E., Domingue, D., Schröder, S. E., et al. 2020, A&A, 639, A83
Watanabe, S., Tsuda, Y., Yoshikawa, M., et al. 2017, Space Sci. Rev., 208, 3
Watanabe, S., Hirabayashi, M., Hirata, N., et al. 2019, Science, 364, 268
Zou, X.-D., Li, J.-Y., Clark, B. E., et al. 2021, Icarus, 358, 114183